Sensitive Detection of Mediastinal Lymph Node Metastasis of Lung Cancer with ^{11}C-Choline PET

Toshihiko Hara, Keizo Inagaki, Noboru Kosaka, and Toyohiko Morita

Departments of Radiology, Chest Surgery, and Pathology, International Medical Center of Japan, Tokyo, Japan

^{11}C-choline and FDG are PET tracers used to visualize various malignancies. In this study, we compared their capabilities in detecting mediastinal lymph node metastasis originating from non–small cell lung cancer (NSCLC). **Methods:** Twenty-nine patients with biopsy-proven NSCLC were studied with PET. ^{11}C-choline PET and FDG PET were performed from 5 and 40 min, respectively, after injection of 370 MBq tracer. PET data were analyzed in terms of the standardized uptake value (SUV). After the PET study, the patients underwent lung resection and mediastinal lymph node dissection. The resected specimens were examined pathologically, and the PET data were analyzed in reference to the pathologic data. **Results:** With ^{11}C-choline, the SUV in metastasis was similar to the SUV in the primary tumor, where the similarity of the SUV was 100% allowing for a 40% difference. With FDG, small metastases were invisible on the PET image. The SUV of FDG in metastasis was much smaller than that in the primary tumor, and the similarity of the SUV was only 19% allowing for a 40% difference. When pathologic findings were used as standards, the sensitivities of ^{11}C-choline PET and FDG PET in detecting mediastinal lymph node metastasis were 100% and 75%, respectively. **Conclusion:** ^{11}C-choline PET was very effective in detecting lymph node metastases in the mediastinum originating from NSCLC, with a sensitivity of 100%. ^{11}C-choline PET promises to be useful not only before surgery but also after surgery.

Key Words: PET; ^{11}C-choline; FDG; lung cancer; staging

J Nucl Med 2000; 41:1507–1513

Complete resection is the ultimate goal of surgery for non–small cell lung cancer (NSCLC) (*1*). Since the pioneering work of Cahan et al. (2) in 1951, mediastinal lymph node dissection has been a part of lung cancer resection. However, the lymph node dissection has been understood with contradictory meanings: excision of easily accessible lymph nodes for pathologic staging (lymph node sampling) and extended lymph node excision with a goal of complete cure (radical lymphadenectomy) (*1*). In practice, many surgeons take an intermediate approach (ordinary lymph node dissection). Radical lymphadenectomy is a rather difficult procedure, which requires precise localization of mediastinal lymph node metastasis to select the optimal surgical procedure (by what route and to what extent) (*1,3*). The noninvasive methods of mediastinal lymph node staging currently used are CT and FDG PET (*4–7*). Although these methods have been reported to provide a relatively high accuracy in identifying metastatic disease, there remains a substantial number of patients who are found to have advanced disease at surgery. Furthermore, not all lymph node metastases are detected at the time of surgical and pathologic evaluation (sampling error) (*8*).

Recently, we developed a new PET tracer, ^{11}C-choline, for tumor detection (*9–13*). Choline, a kind of vitamin, is incorporated in normal and tumor cells in the body and is used in various ways. The only metabolic pathway of choline in tumor cells is its conversion into phosphorylcholine followed by synthesis of phosphatidylcholine, which finally constitutes the main component of cell membranes (*14–16*). Because tumor cells duplicate very quickly, the biosynthesis of cell membranes is also very fast. Consequently, the uptake of ^{11}C-choline in tumors represents the rate of tumor cell duplication.

We performed both ^{11}C-choline PET and FDG PET in 29 patients with resectable NSCLC. Resected tissues underwent pathologic examination after surgery. The accuracy of ^{11}C-choline PET, FDG PET, and CT in lymph node staging was evaluated by comparing imaging data with pathologic findings. At the initial stage of this study, surgeons estimated the extent of mediastinal lymph node metastasis using CT and FDG PET. However, at a later stage of the study, surgeons relied most on ^{11}C-choline PET.

MATERIALS AND METHODS

Phantom Study to Quantitate Radioactive Spots of Small Size

Teflon tubing of various inner diameters was packed with ^{18}F-containing water at a constant radioactivity concentration (37 MBq/L), suspended in air or in water (using a 20-cm-diameter water cylinder in the latter case), and placed within the field of view of a PET camera; these tubings were then scanned in the ordinary way by PET (scan time, 3 min). The emission data were attenuation corrected using transmission data. The radioactivity concentration exhibited on the computer screen was compared with the true radioactivity concentration measured in a well counter (the PET camera and the well counter were previously cross-calibrated using a 20-cm-diameter water cylinder containing ^{18}F).

Received Jul. 13, 1999; revision accepted Jan. 19, 2000.

For correspondence or reprints contact: Toshihiko Hara, MD, PhD, Department of Radiology, International Medical Center of Japan, 1-21-1 Toyama, Shinjuku-ku, Tokyo 162, Japan.

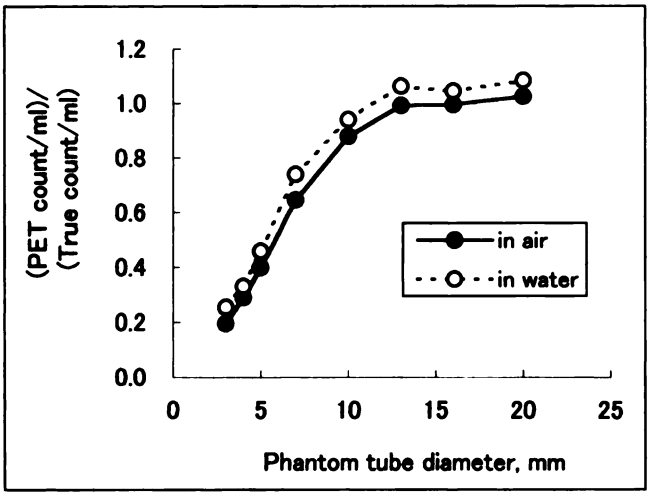

FIGURE 1. Phantom study shows quantitation of PET image. ^{18}F-containing solution at constant radioactivity concentration was packed in Teflon tubing of various inner diameters, suspended in air or in water (water cylinder of 20-cm diameter). PET scan was performed, and radioactivity concentration exhibited on computer screen was compared with true radioactivity concentration determined using well counter.

Patients

Twenty-nine patients (19 men, 10 women; mean age, 65.1 y; age range, 43–80 y) with biopsy-proven NSCLC and mediastinal lymph node metastases regarded as N0 (no metastasis), N1 (ipsilateral peribronchial and hilar), or N2 (ipsilateral mediastinal and subcarinal) on CT were studied with ^{11}C-choline PET and FDG PET after informed consent was obtained. The histologic types were adenocarcinoma (n = 13), squamous cell carcinoma (n = 10), adenosquamous cell carcinoma (n = 4), large cell carcinoma (n = 1), and bronchioloalveolar carcinoma (n = 1). The tumor extents were T1 (n = 15), T2 (n = 13), and T3 (n = 1) on the basis of the TNM classification (*17*). After PET studies, all patients underwent lung resection, and resected specimens were examined by experienced pathologists.

PET Scan and Data Analysis

^{11}C-choline (*18*) and FDG (*19*) were prepared using a cyclotron and automated synthetic apparatus that we constructed. PET scanning was performed in the morning after the patient had fasted overnight. The PET camera (Headtome IV, 6-mm spatial resolution; Shimadzu, Kyoto, Japan) was equipped with 3 rings of bismuth germanate (BGO) detectors to produce 5 slices at 13-mm intervals. In the case of ^{11}C-choline PET, when the transmission scan was obtained, ^{11}C-choline (370 MBq) was injected, and emission scanning was started 5 min after injection. In the case of FDG PET, when transmission scanning finished, FDG (370 MBq) was injected, and emission scanning was started 40 min after injection. Both the transmission and the emission scans were

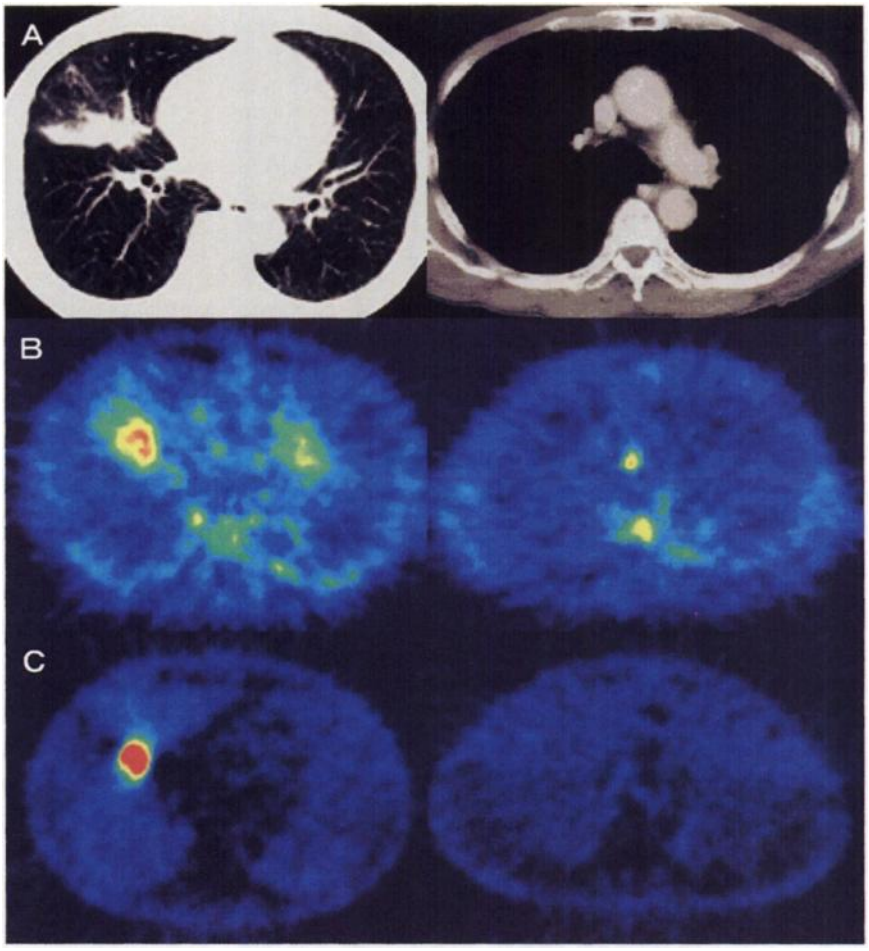

FIGURE 2. Primary tumor and mediastinal lymph node metastasis shown by CT (A), ^{11}C-choline PET (B), and FDG PET (C) of patient 7 (Table 1). Left images show primary tumor, and right images show metastasis. Metastasis was obvious only with ^{11}C-choline PET.

obtained from the liver to the neck, by shifting the bed position 6 times, with a scan time of 3 min each. By combining the transmission and emission data in a computer, attenuation-corrected emission images (PET images) were obtained. A series of horizontal images were displayed on the computer screen in color.

Using a color scale, the radioactivity concentration in each pixel (4 × 4 × 9.5 mm in real size) was displayed in terms of the standardized uptake value (SUV), where SUV represents (regional radioactivity concentration/[total injected dose/body weight]). Numeric values for the SUV in regions of interest were also displayed. The ^{11}C-choline image and FDG image were reviewed by a group of radiologists who had no knowledge beyond the localization of the primary tumor. In the case of ^{11}C-choline images, the reading was easy: Any radioactive area of the SUV similar to that of the primary tumor was considered to be metastasis (allowing for a 40% difference in the SUV). A high uptake in bone marrow of the vertebra, appearing at constant intervals from slice to slice, was ignored. The localization of the metastasis was determined by the distance from the diaphragm in reference to CT films. In the case of FDG images, the reading was more difficult: The SUV in the metastasis was always far less than the SUV in the primary tumor, and the SUV was often <1.0 (the area of the SUV < 1.0 was indistinct from background). When FDG uptake was indistinct but ^{11}C-choline uptake was distinct, the SUV for FDG was measured at the spot identical to that at which ^{11}C-choline uptake was distinct.

Surgery and Pathologic Examination of Resected Specimens

The patients underwent lobectomy or pneumonectomy through a posterolateral incision (standard thoracotomy) or a sternal incision (median sternotomy). Most patients underwent standard thoracotomy and ordinary lymph node dissection. The lymph node dissection was performed as follows. The connective tissue surrounding the trachea and aorta was removed together with lymph nodes. Dissection was performed only on the side ipsilateral to the incision. The contralateral side and other inaccessible regions were ignored. A more extended dissection was performed in 1 patient undergoing median sternotomy. The surgical specimens were submitted for pathologic examination after fixation in formalin, embedding in paraffin, slicing on a microtome, and staining with hematoxylin and eosin. If lymph node metastases were found on the hematoxylin and eosin slides, the long axis of the node was measured, and the localization was recorded according to the TNM classification (*17*). It is possible that the actual size in vivo of such lymph nodes might have been larger than that measured on the hematoxylin and eosin slides.

RESULTS

The capability of our PET camera to quantitatively estimate the radioactivity concentration within a small radioactive spot was examined by a phantom study. As shown in Figure 1, the quantitation was achieved only if the

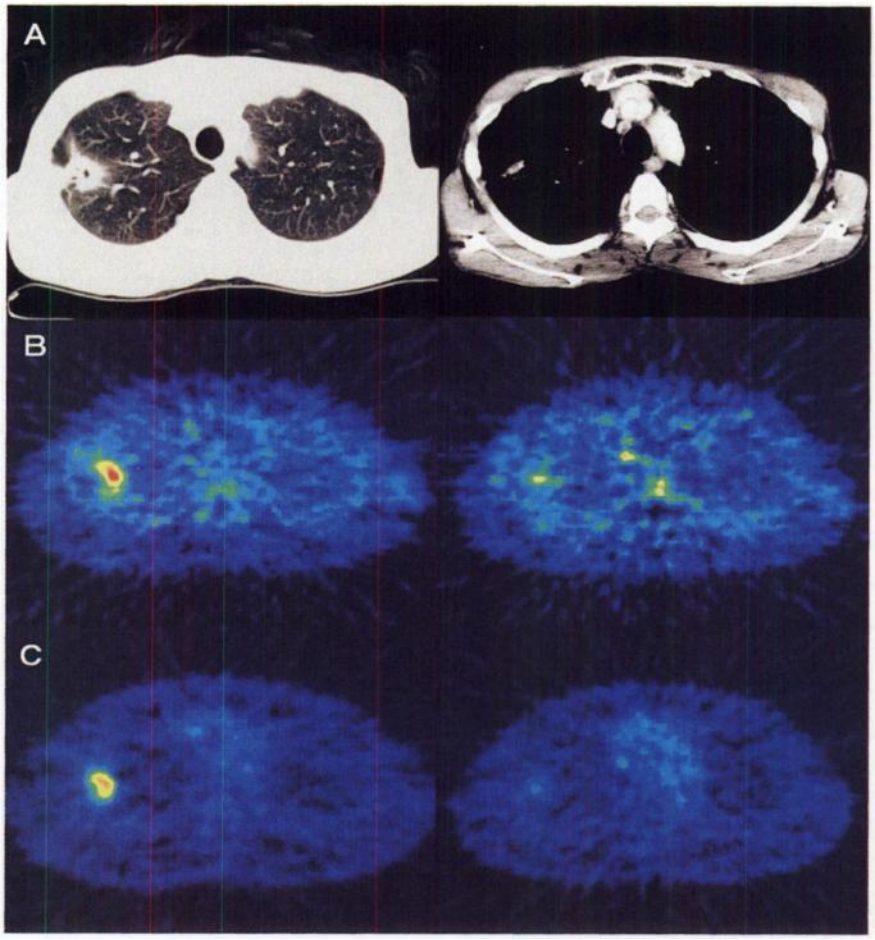

FIGURE 3. Primary tumor and mediastinal lymph node metastasis shown by CT (A), ^{11}C-choline PET (B), and FDG PET (C) of patient 10 (Table 1). Left images show primary tumor, and right images show metastasis. Metastasis was obvious only with ^{11}C-choline PET.

diameter of the radioactive spot was >13 mm. If the diameter was 7 mm, the apparent radioactivity concentration exhibited on the PET camera screen was 65%–75% of the true radioactivity concentration (measured in a well counter).

Typical cases of NSCLC studied by CT, ^{11}C-choline PET, and FDG PET are presented in Figures 2–4, where an equal color scale is used for each pair of PET images so that the SUV in the primary tumor and the SUV in metastases can be compared. Cumulative results from the 29 patients are given in Table 1.

With ^{11}C-choline, the SUV in metastases was similar to the SUV in the primary tumor, usually within a difference of 40%. The similarity of the SUV in metastases to the SUV in the primary tumor was 100%, allowing for a 40% difference.

With FDG, the SUV in metastases was much smaller than the SUV in the primary tumor. With FDG, small metastases were not visible on the PET image. There was almost no similarity between the SUV of FDG in metastases and the SUV in the primary tumor. The similarity was only 19%, allowing for a 40% difference.

In the ^{11}C-choline PET image, any small area that showed a SUV similar to the SUV of the primary tumor was considered to be metastasis. This tentative diagnosis was reappraised pathologically, and it was shown that all metastases detected on pathologic examination were also visualized with ^{11}C-choline PET. This high sensitivity of detecting mediastinal lymph node metastasis with ^{11}C-choline may be partially ascribed to the conglomeration of multiple metastatic lymph nodes, as is observed frequently in pathologic specimens (Table 1).

Identification of metastases was rather difficult on the FDG PET image, but we measured the SUV of possible metastatic sites using information from the ^{11}C-choline image. Table 2 shows the sensitivity, specificity, and accuracy of CT, ^{11}C-choline PET, and FDG PET in finding mediastinal lymph node metastasis in 29 patients with NSCLC, where all lymph node stations from station 1 to station 9 (n = 261) were analyzed. The lymph nodes showing an SUV > 1.0 were considered positive and were used in this analysis (other lymph nodes were indistinguishable from background). It was obvious that ^{11}C-choline PET was superior to CT and FDG PET in detecting mediastinal lymph node metastasis from NSCLC. A discrepancy between pathologic and PET findings (pathologically negative and false-positive on both ^{11}C-choline PET and FDG PET) was observed in a group of lymph node stations that could be easily overlooked at surgery. The specificity and accuracy of ^{11}C-choline PET and FDG PET would increase if there were no such sampling errors.

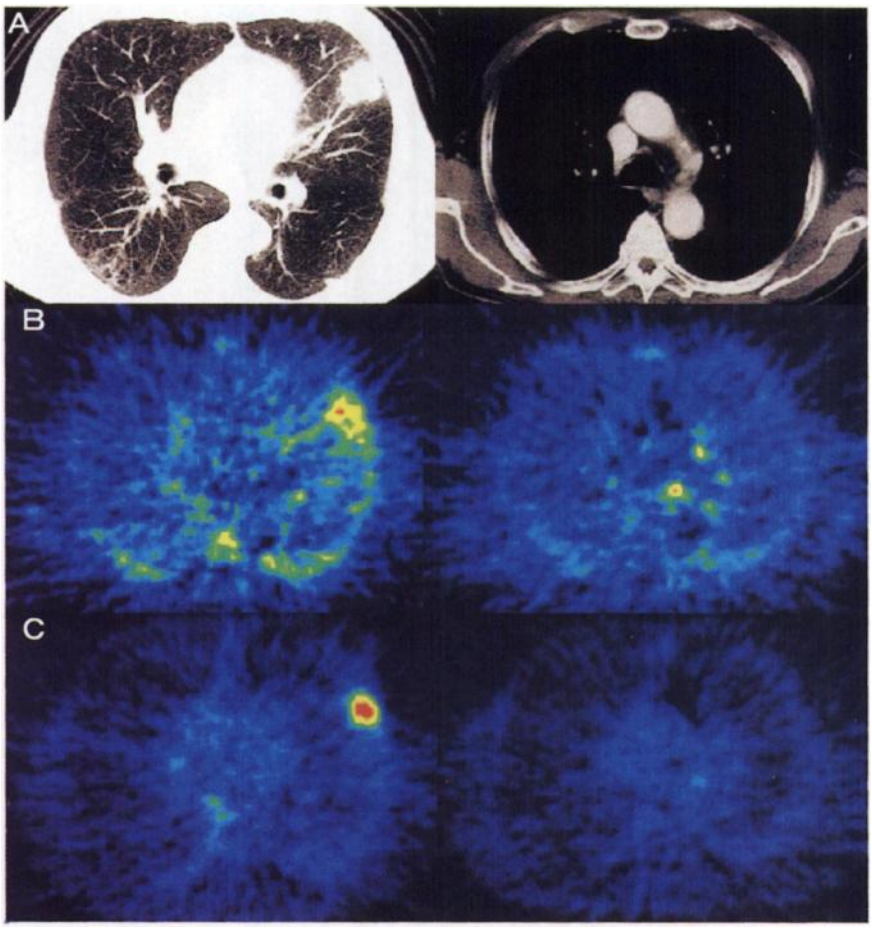

FIGURE 4. Primary tumor and mediastinal lymph node metastasis shown by CT (A), ^{11}C-choline PET (B), and FDG PET (C) of patient 20 (Table 1). Left images show primary tumor, and right images show metastasis. Metastasis was obvious only with ^{11}C-choline PET.

TABLE 1
Primary Tumor and Mediastinal Lymph Node Metastasis in NSCLC Determined by Pathology, CT, ^{11}C-Choline PET, and FDG PET

Patient no.	Histology	Pathology: Tumor Site	Pathology: Tumor Size (mm)	Pathology: Node Site	Pathology: Node Size (mm)	CT: Node size (mm)	^{11}C-choline PET: Tumor SUV	^{11}C-choline PET: Node SUV	FDG PET: Tumor SUV	FDG PET: Node SUV
1	Mod sq	$IS_{8,9}$	56	—	—	—	4.21	—	5.26	—
2	Poor ad-sq	rS_6	28	10	9 (×1)	—	1.36	1.56	1.70	0.54
3	Poor sq	IS_{1+2}	29	1	—	—	1.73	1.79	4.41	1.02
				7	—	—		1.86		1.57
4	Mod ad	rS_2	18	—	—	—	2.39	—	3.72	—
5	Well ad	rS_2	12	—	—	—	1.98	—	1.76	—
6	Mod sq	rS_8	45	—	—	—	2.59	—	3.12	—
7	Poor sq	rS_4	36	3	3 (×3)	18	1.63	1.23	1.91	0.27
				7	13 (×2)	—		1.14		0.49
8	Mod sq	IS_{1+2}	33	—	—	—	3.21	—	3.76	—
9	Mod sq	IS_3	19	7	12 (×1)	—	3.21	3.26	2.30	2.52
10	Mod ad	rS_1	32	2	8 (×3)	—	2.02	1.66	2.30	0.94
				3	4 (×4)	16		1.55		1.01
11	Mod ad-sq	rS_2	33	3	—	18	3.78	—	5.06	—
12	Well ad	rS_1	21	10	—	10	2.44	—	1.70	—
13	Large	IS_9	17	3	—	15	2.20	—	2.01	—
				r8	—	—		3.60		1.40
				10	20 (×1)	—		2.06		2.23
14	Well ad	rS_2	22	2	—	—	3.74	3.19	3.28	1.14
				3	2 (×3)	13		3.50		1.42
				7	—	—		3.33		1.55
15	Bronch-alv	IS_8	140	—	—	—	2.16	—	1.87	—
16	Well ad-sq	rS_{1+2}	18	5	5 (×1)	—	3.24	2.78	2.26	1.24
				10	12 (×1)	—		2.41		1.27
17	Mod sq	IS_3	35	7	—	—	5.79	3.40	5.99	1.69
18	Mod sq	IS_3	19	—	—	—	1.75	—	1.80	—
19	Well ad-sq	rS_6	53	—	—	—	3.46	—	10.12	—
20	Mod ad	IS_4	31	4	6 (×1)	—	2.48	2.83	2.83	1.01
				5	6 (×1)	—		2.57		1.31
21	Well ad	IS_8	33	—	—	—	3.95	—	3.29	—
22	Mod ad	IS_6	85	—	—	—	4.16	—	3.67	—
23	Mod ad	rS_4	19	7	7 (×1)	—	1.64	1.51	1.41	1.40
24	Mod ad	IS_{1+2}	23	—	—	—	4.07	—	3.34	—
25	Well ad	rS_3	49	—	—	—	2.66	—	1.55	—
26	Mod sq	IS_6	25	10	6 (×1)	—	3.34	2.98	3.18	1.49
				r10	—	—		3.58		1.37
27	Mod ad	rS_6	19	—	—	—	3.19	—	1.17	—
28	Mod ad	rS_6	34	1	2 (×2)	—	2.85	2.92	3.58	1.02
				3	3 (×3)	—		2.40		1.21
29	Poor sq	rS_3	21	—	—	—	2.44	—	2.22	—

mod = moderately differentiated; sq = squamous cell carcinoma; poor = poorly differentiated; ad-sq = adenosquamous cell carcinoma; ad = adenocarcinoma; well = well differentiated; large = large cell carcinoma; bronch-alv = bronchioloalveolar carcinoma.

Tumor site is presented according to pulmonary segment anatomy. Lymph node site with metastasis is presented according to lymph node station numbering of TNM classification (*17*) (mediastinal = 1–9, hilar = 10). Pathologic and CT size is presented by long-axis distance (mm). Conglomeration of metastatic lymph nodes found on pathologic examination is presented within parentheses (×..) after largest size of them. Radioactivity uptake is presented by SUV. Lymph node metastasis of SUV < 1.0 was invisible on PET image.

DISCUSSION

We previously introduced ^{11}C-choline PET for imaging brain tumor, lung cancer, esophageal cancer, colon cancer, prostate cancer, bladder cancer, and their metastases (*9–13*). ^{11}C-choline PET is effective in detecting both primary (large) and metastatic (small) tumors (giving similar SUVs), making a sharp contrast to FDG PET, which is highly sensitive (high SUV) to primary tumors but far less sensitive (very low SUV) to metastatic tumors. The difference in these sensitivity characteristics can be explained as follows. A high uptake of FDG in tumors is accomplished only if the tumor metabolism is biased toward excessive glycolysis by

TABLE 2
Sensitivity, Specificity, and Accuracy of CT, ^{11}C-Choline PET, and FDG PET in Finding Mediastinal Lymph Node Metastasis in 29 Patients with NSCLC

Parameter	CT	^{11}C-choline PET	FDG PET
Sensitivity (%)	19	100	75
Specificity (%)	99	97	97
Accuracy (%)	94	97	96

Analysis was performed for all lymph node stations from station 1 to station 9 (n = 261). Only lymph nodes with SUV > 1.0 were considered positive in this analysis.

activation of the glucose transporter and hexokinase (*20–23*). This may occur, although there seem to be rare exceptions, if the tumor size is large and the tumor environment is hypoxic because of insufficient blood (oxygen) supply. In contrast, the uptake of ^{11}C-choline in tumors is the result of cell membrane synthesis: the higher the tumor proliferation, the higher the cell membrane synthesis. When ^{11}C-choline is incorporated in tumors, it is rapidly phosphorylated (yielding ^{11}C-phosphorylcholine) and chemically trapped inside the cell membranes. ^{11}C-phosphorylcholine may be the major chemical form derived from ^{11}C-choline at the time of PET scanning. Thereafter, it is further metabolized and converted to ^{11}C-phosphatidylcholine and then integrated in tumor cell membranes (*12–18*). This is the only metabolic pathway known for choline in tumors, although there are other metabolic pathways in other normal organs (i.e., synthesis of acetylcholine and betaine). Therefore, it can be assumed that the ^{11}C-choline uptake in tumors is proportional to the tumor cell proliferation rate.

The similarity in the intensity of ^{11}C-choline uptake between primary tumor and metastases, as observed in this study, can be explained by the similarity in tumor cell proliferation rates. Monoclonality is the fundamental characteristic of neoplasia (*24*). The identity of clonality in multiple tumors has been confirmed in patients with breast cancer (*25*) and bladder cancer (*26*) using the methods of molecular genetics. However, during a long span of tumor cell generations, a genetic change may occur, and polyclonality will result. If the genetic change is not profound and critical, the proliferation rate may not change much. Studies of patients with gastric cancer (*27*) and colorectal cancer (*27,28*), using the bromodeoxyuridine uptake method, have shown that the proliferation rates of the primary tumor and metastases were similar to each other. All of these findings seem to correspond with our findings that the ^{11}C-choline uptake rates in the primary tumor and metastases were similar in NSCLC.

At surgery for NSCLC (lung resection and lymphadenectomy), some of the lymph node metastases may remain in the mediastinum, particularly if they are small or localized in regions of difficult access (sampling error). The 29 patients in this study whose cancer was diagnosed by CT as N0 (n = 22), N1 (n = 0), or N2 (n = 7) had diagnoses by ^{11}C-choline PET as N0 (n = 15), N1 (n = 1), N2 (n = 11), or N3 (n = 2) and by pathology as N0 (n = 17), N1 (n = 2), or N2 (n = 10). The discrepancy between the ^{11}C-choline PET data and the pathology data seems to be the result of sampling error. It should be emphasized, however, that these residual tumors could be treated effectively by radiotherapy because small tumors and well-oxygenated tumors are highly sensitive to radiation (*29–31*). The first randomized trial of external radiotherapy after resection of NSCLC was undertaken in clinically N2-negative patients, but the survival rate was even worse in the irradiated group because of severe radiation-induced complications (*32*). Subsequent randomized trials in stage II and stage III (N1 and N2) NSCLC (squamous cell carcinoma) showed that the incidence of local recurrence was significantly lower in the irradiated group, but the survival rate was not improved (*33,34*). Another randomized trial in stage IIIa (N2) NSCLC showed a lower incidence of local recurrence as well as a longer survival in the irradiated group (*35*). Recently, Smolle-Juettner et al. (*36*) reported that the NSCLC patient group (with N0, N1, and N2 disease) treated by surgery and postoperative radiotherapy showed a lower incidence of local recurrence in the mediastinum (5/83) than that of the nonirradiated patient group (17/72) ($P < 0.01$), but distant metastases occurred both in the irradiated group (32/83) and in the nonirradiated group (38/72). It has been suggested repeatedly that in completely resected N2 disease, postoperative irradiation will lead to an improved survival rate, implying that not all patients with subclinical N2 disease develop distant metastases (*37–40*). At the time of postoperative irradiation, it is necessary to confine the irradiated area to the malignancy and avoid unnecessary irradiation because lung function in these patients is already compromised. In this setting, postoperative ^{11}C-choline PET will provide information about whether the radiotherapy is truly necessary and which part of the mediastinum, if any, needs irradiation. ^{11}C-choline PET performed 3 wk after surgery is not influenced by the effect of previous surgery (*9*).

CONCLUSION

^{11}C-choline PET was very effective in detecting mediastinal lymph node metastases of NSCLC, with a sensitivity of 100%. This procedure will be useful in selecting the most effective surgical procedure for treatment of NSCLC. However, residual tumors (metastases) may remain in the mediastinum after surgery. ^{11}C-choline PET also promises to be useful if postsurgical radiotherapy is being considered.

ACKNOWLEDGMENTS

This work was supported in part by the Science and Technology Agency of Japan and the Japanese Smoking Research Foundation.

REFERENCES

1. Ginsberg RJ. Resection of non-small cell lung cancer: how much and by what route. *Chest*. 1997;112(suppl):203S–205S.
2. Cahan WG, Watson WL, Pool JL. Radical pneumonectomy. *J Thorac Cardiovasc Surg*. 1951;22:449–473.
3. Izbicki JR, Passlick B, Pantel K, et al. Effectiveness of radical systematic mediastinal lymphadenectomy in patients with resectable non-small cell lung cancer: results of a prospective randomized trial. *Ann Surg*. 1998;227:138–144.
4. Patz EF Jr, Lowe VJ, Goodman PC, Herndon J. Thoracic nodal staging with PET imaging with ^{18}FDG in patients with bronchogenic carcinoma. *Chest*. 1995;108: 1617–1621.
5. Scott WJ, Gober LS, Terry JD, Dewan NA, Sunderland JJ. Mediastinal lymph node staging of non-small-cell lung cancer: a prospective comparison of computed tomography and positron emission tomography. *J Thorac Cardiovasc Surg*. 1996;111:642–648.
6. Bury T, Paulus P, Dowlati A, et al. Staging of the mediastinum: value of positron emission tomography imaging in non-small cell lung cancer. *Eur Resp J*. 1996;9:2560–2564.
7. Vansteenkiste JF, Stroobauts SG, De Leyn PR, et al. Mediastinal lymph node staging with FDG-PET scan in patients with potentially operable non-small cell lung cancer: a prospective analysis of 50 cases. *Chest*. 1997;112:1480–1486.
8. Sawyer TE, Bonner JA, Gould PM, et al. Predictors of subclinical nodal involvement in clinical stages I and II non-small cell lung cancer: implications in the inoperable and three-dimensional dose-escalation settings. *Int J Radiat Oncol Biol Phys*. 1999;43:965–970.
9. Hara T, Kosaka N, Shinoura N, Kondo T. PET imaging of brain tumor with [*methyl*-^{11}C]choline. *J Nucl Med*. 1997;38:842–847.
10. Hara T, Kosaka N, Kishi H. PET imaging of prostate cancer using carbon-11-choline. *J Nucl Med*. 1998;39:990–995.
11. Hara T, Kosaka N, Kondo T, Kishi H, Kobori O. Imaging of brain tumor, lung cancer, esophagus cancer, colon cancer, prostate cancer, and bladder cancer with [C-11]choline [abstract]. *J Nucl Med*. 1997;38(suppl):250P.
12. Inagaki K, Morita T, Fujii K, Kosaka N, Hara T. Mediastinal lymph node staging in non-small cell lung cancer using PET with C-11 choline and F-18 FDG [abstract]. *J Nucl Med*. 1999;40(suppl):59P–60P.
13. Kobori O, Kirihara Y, Kosaka N, Hara T. Positron emission tomography of esophageal carcinoma using ^{11}C-choline and ^{18}fluorodeoxyglucose: a novel method of preoperative lymph node staging. *Cancer*. 1999;86:1638–1648.
14. Ronen SM, Rushkin E, Degani H. Lipid metabolism in T47D human breast cancer cells: ^{31}P and ^{13}C-NMR studies of choline and ethanolamine uptake. *Biochim Biophys Acta*. 1991;1095:5–16.
15. Katz-Brull R, Degani H. Kinetics of choline transport and phosphorylation in human breast cancer cells: NMR application of the zero trans method. *Anticancer Res*. 1996;16:1375–1380.
16. Aiken NR, Gillies RJ. Phosphomonoester metabolism as a function of all proliferative status and exogenous precursors. *Anticancer Res*. 1996;16:393–397.
17. Hermanek P, Hutter RVP, Sobin LU, Wagner G, Wittekind C, eds. *TNM Atlas: Illustrated Guide to the TNM/pTNM Classification of Malignant Tumours*. 4th ed. Berlin, Germany: Springer; 1997:153–155.
18. Hara T, Yuasa M. Automated synthesis of [^{11}C]choline, a positron-emitting tracer for tumor imaging. *Appl Radiat Isot*. 1999;50:531–533.
19. Yuasa M, Yoshida H, Hara T. Computer-controlled synthesis of [^{18}F]FDG by the tetrabutylammonium method: achievement of high yield, purity, reproducibility, reliability, and safety. *Appl Radiat Isot*. 1997;48:201–205.
20. Clavo AC, Brown RS, Wahl RL. Fluorodeoxyglucose uptake in human cancer cell lines is increased by hypoxia. *J Nucl Med*. 1995;36:1625–1632.
21. Minn H, Clavo AC, Wahl RL. Influence of hypoxia on tracer accumulation in squamous-cell carcinoma: in vitro evaluation for PET imaging. *Nucl Med Biol*. 1996;23:941–946.
22. Gulledge CJ, Dewhirst MW. Tumor oxygenation: a matter of supply and demand. *Anticancer Res*. 1996;16:741–749.
23. Muthupala SP, Rempel A, Pedersen PL. Aberrant glycolytic metabolism of cancer cells: a remarkable coordination of genetic, transcriptional, post-translational, and mutational events that lead to a critical role for type II hexokinase. *J Bioenerg Biomembr*. 1997;29:339–343.
24. Friberg S, Mattson S. On the growth rates of human malignant tumors: implications for medical decision making. *J Surg Oncol*. 1997;65:284–297.
25. Noguchi S, Aihara T, Koyama H, Motomura K, Inaji H, Imaoka S. Discrimination between multicentric and multifocal carcinomas of the breast through clonal analysis. *Cancer*. 1994;74:872–877.
26. Sidransky D, Frost P, Von Eschenbach A, Oyasu R, Preisinger AC, Vogelstein B. Clonal origin of bladder cancer. *N Engl J Med*. 1992;326:737–740.
27. Shimomatsuya T, Tanigawa N, Muraoka R. Proliferative activity of human tumors: assessment using bromodeoxyuridine and flow cytometry. *Jpn J Cancer Res*. 1991;82:357–362.
28. Ooyama S, Yamaguchi A, Yonemura Y, et al. Metastasis and its relation to cell kinetics in human colorectal cancers [in Japanese]. *Nippon Geka Gakkai Zasshi*. 1990;91:677–682.
29. Moulder JE, Rockwell S. Hypoxic fractions of solid tumors: experimental techniques, methods of analysis, and a survey of existing data. *Int J Radiat Oncol Biol Phys*. 1984;10:695–712.
30. Gatenby RA, Kessler HB, Rosenblum JS, et al. Oxygen distribution in squamous cell carcinoma metastases and its relationship to outcome of radiation therapy. *Int J Radiat Oncol Biol Phys*. 1988;14:831–838.
31. Hockel M, Vorndran B, Schlenger K, Baussmann E, Knapstein PG. Tumor oxygenation: a new predictive parameter in locally advanced cancer of the uterine cervix. *Gynecol Oncol*. 1993;51:141–149.
32. Van Houtte PV, Rocmans P, Smets P. Postoperative radiation therapy in lung cancer: a controlled trial after resection of curative design. *Int J Radiat Oncol Biol Phys*. 1980;6:983–986.
33. Lung Cancer Study Group. Effects of postoperative mediastinal radiation on completely resected stage II and stage III epidermoid cancer of the lung. *N Engl J Med*. 1986;315:1377–1381.
34. Neptune WB. Primary lung cancer surgery in stage II and III. *Arch Surg*. 1988;123:583–585.
35. Astudillo J, Conill C. Role of postoperative radiation therapy in stage IIIa non-small cell lung cancer. *Ann Thorac Surg*. 1990;50:618–623.
36. Smolle-Juettner FM, Mayer R, Pinter H, et al. "Adjuvant" external radiation of the mediastinum in radically resected non-small cell lung cancer. *Eur J Cardiothorac Surg*. 1996;10:947–950.
37. Choi NC, Grillo HC, Gardiello M, et al. Basis for new strategies in postoperative radiotherapy of bronchogenic carcinoma. *Int J Radiat Oncol Biol Phys*. 1980;6: 31–35.
38. Medical Research Council Lung Cancer Working Party. The role of post-operative radiotherapy in non-small-cell lung cancer: a multicentre randomized trial in patients with pathologically staged T_{1-2}, N_{1-2}, M_0 disease. *Br J Cancer*. 1996; 74:632–639.
39. Weisenberger TH. Effects of postoperative mediastinal radiation on completely resected stage II and stage III epidermoid cancer of the lung: LCSG 773. *Chest*. 1994;106(suppl 6):297S–301S.
40. Sawyer TE, Bonner JA, Gould PM, et al. The impact of surgical adjuvant thoracic radiation therapy for patients with nonsmall cell lung carcinoma with ipsilateral mediastinal lymph node involvement. *Cancer*. 1997;80:1399–1408.